





Brillouin Klein bottle from artificial gauge fields

Z. Y. Chen¹, Shengyuan A. Yang²  & Y. X. Zhao^{1,3}  

A Brillouin zone is the unit for the momentum space of a crystal. It is topologically a torus, and distinguishing whether a set of wave functions over the Brillouin torus can be smoothly deformed to another leads to the classification of various topological states of matter. Here, we show that under \mathbb{Z}_2 gauge fields, i.e., hopping amplitudes with phases ± 1 , the fundamental domain of momentum space can assume the topology of a Klein bottle. This drastic change of the Brillouin zone theory is due to the projective symmetry algebra enforced by the gauge field. Remarkably, the non-orientability of the Brillouin Klein bottle corresponds to the topological classification by a \mathbb{Z}_2 invariant, in contrast to the Chern number valued in \mathbb{Z} for the usual Brillouin torus. The result is a novel Klein bottle insulator featuring topological modes at two edges related by a nonlocal twist, radically distinct from all previous topological insulators. Our prediction can be readily achieved in various artificial crystals, and the discovery opens a new direction to explore topological physics by gauge-field-modified fundamental structures of physics.

¹National Laboratory of Solid State Microstructures and Department of Physics, Nanjing University, Nanjing 210093, China. ²Research Laboratory for Quantum Materials, Singapore University of Technology and Design, Singapore 487372, Singapore. ³Collaborative Innovation Center of Advanced Microstructures, Nanjing University, Nanjing 210093, China. email: zhaoyx@nju.edu.cn

The Brillouin zone is a fundamental concept in physics. It is essential for the physical description of crystalline solids, metamaterials, and artificial periodic systems. Particularly, it sets the stage for classifying topological states, which, in mathematical terms, is the task to study the topology of Hermitian vector bundles over the Brillouin zone as the base manifold^{1–3}. Clearly, the topology of the Brillouin zone itself is a crucial ingredient for the classification. Since Brillouin zones have the topology of a torus, topological states known to date basically correspond to classifications done on the torus.

Meanwhile, although initially studied for electronic systems in solids^{4–6}, topological states have been successfully extended to artificial crystals, such as acoustic/photonic crystals, electric circuit arrays, and mechanical networks. These systems have the advantage of great tunability. More importantly, gauge fields can be flexibly engineered in artificial crystals. In particular, the \mathbb{Z}_2 gauge field, i.e., hopping amplitudes allowed to take phases ± 1 , can be readily realized in these systems and have already been demonstrated in many experiments^{7–17}. A crucial but so far less appreciated point is that under gauge fields, symmetries of the system would satisfy projective algebras^{18–21} beyond the textbook group theory for crystal symmetry²², which has recently been experimentally demonstrated by acoustic crystals^{23,24}. Then, what is the physical consequence of the projective symmetry algebra? Does it generate any new topology that is impossible for systems without gauge field? These questions have not been answered yet.

In this article, we reveal that the projective symmetry algebra can lead to a fundamental change of the Bloch band theory. We show that it can generate a peculiar “momentum-space nonsymmorphic symmetry”, i.e., when represented in momentum space, the projective algebra requires that certain symmetry must include a fractional translation in the reciprocal lattice. For example, a real-space reflection symmetry can become a glide reflection in momentum space. This unique feature in turn dictates the topology of the fundamental domain of the momentum space being a Klein bottle and leads to new topological states.

Results

Emergent momentum-space glide reflection. Let us start by considering the reflection symmetry M_x that inverts the x axis, and the translation symmetry L_y along the y direction. In the absence of gauge fields, they should commute with each other $[M_x, L_y] = 0$. However, under certain gauge flux configurations, the algebraic relation may be projectively modified to

$$\{M_x, L_y\} = 0, \quad (1)$$

where the font has been changed to indicate the representations under gauge fields. The seemingly peculiar relation in (1) can be intuitively understood by inspecting Fig. 1. Here, we have four lattice sites forming a rectangle invariant under M_x . Assuming there is a \mathbb{Z}_2 gauge flux of π through the rectangle, then both $M_x L_y$ and $L_y M_x$ would send a particle from site 1 to 3, but the two paths enclose a π flux, therefore resulting in the anti-commutation.

For a crystalline system, if we choose a unit cell with lattice constant b along the y direction, the operator L_y is diagonalized as $\hat{L}_y = e^{ik_y b}$ in the momentum space. Then, the projective algebra in Eq. (1) requires

$$\hat{M}_x e^{ik_y b} \hat{M}_x = -e^{ik_y b} = e^{i(k_y + G_y/2)b}, \quad (2)$$

where G_y is the length of the reciprocal lattice vector \mathbf{G}_y . From Eq. (2), we make the key observation that \hat{M}_x must contain a half translation in the reciprocal lattice along k_y , when represented in

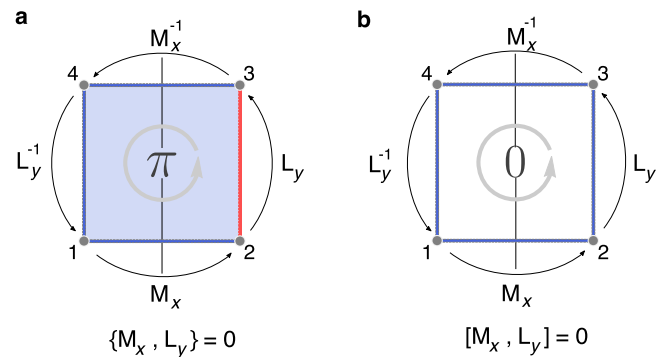


Fig. 1 Flux and symmetry algebra. **a** A rectangle with π flux. Blue/red color indicates hopping amplitudes with positive/negative signs. Successive operations $L_y^{-1} M_x^{-1} L_y M_x$ move a particle around the rectangle, which encloses the π flux, so the result is equal to -1 , leading to the anti-commutation algebra. **b** When there is no flux, M_x and L_y follow the ordinary commutation algebra.

the momentum space. Explicitly,

$$\hat{M}_x = U \mathcal{L}_{\frac{G_y}{2}} \hat{m}_x, \quad (3)$$

where U is some unitary matrix, \hat{m}_x is the operator that inverts k_x and $\mathcal{L}_{G_y/2}$ denotes the operator that implements the half translation $\mathbf{G}_y/2$ of the reciprocal lattice. Hence, M_x may be regarded as a momentum-space glide reflection.

As an example, consider the simple lattice model in Fig. 2a. Here, the primitive unit cell in real space consist of four sites. The \mathbb{Z}_2 gauge flux through each plaquette is specified in the figure, respecting M_x and the translation period of b along y . Evidently, relation Eq. (1) is fulfilled for this case, and the mirror symmetry operator is represented by

$$\hat{M}_x = \tau_0 \otimes \sigma_1 \mathcal{L}_{\frac{G_y}{2}} \hat{m}_x \quad (4)$$

in momentum space, where τ_s and σ_s are two sets of Pauli matrices that operate on rows and columns of a unit cell [see Fig. 2a].

The appearance of the fractional reciprocal lattice translation can also be understood from the following analysis. To describe a lattice with gauge flux, we need to choose explicit gauge connections on the lattice bonds. For instance, in Fig. 2a, we show a specific gauge choice, with red and blue colors denoting negative and positive hopping amplitudes, respectively. Then, for this given gauge choice, a crystal symmetry operator is given by $\mathbf{R} = \mathbf{G}\mathbf{R}$, namely a combination of the manifest spatial operator R and a gauge transformation \mathbf{G} . This is because although the flux configuration is invariant under R , the specific gauge connection configuration may be changed by R . To restore the original gauge connection, an additional gauge transformation \mathbf{G} should be performed. For instance, the gauge transformation required after reflection M_x is depicted in Fig. 2b. Notably, \mathbf{G} may not be compatible with the spatial period of the lattice. [Here, it must be incompatible with L_y due to Eq. (1).] Clearly, in Fig. 2b, the period of \mathbf{G} along y doubles the lattice constant. Then, after Fourier transform, the incompatibility manifests in M_x as a fractional translation in momentum space.

Note that for conventional space groups, nonsymmorphic symmetries such as glide reflections exist only on real-space lattices, i.e., the involved fractional translations act only in real space but not in momentum space^{25,26}. When transformed to momentum space, they invariably become fixed-point operations, namely, there are always momenta (such as the Γ point) that are invariant under the operation. Therefore, ordinary (real-space)

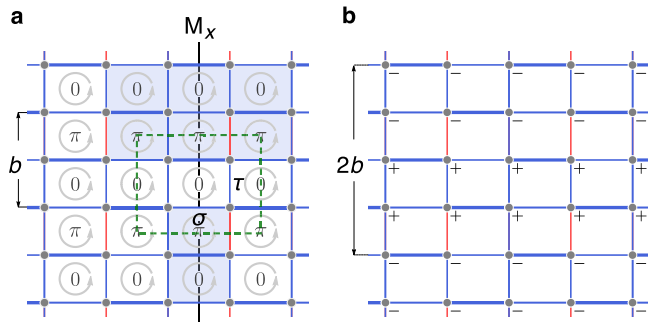


Fig. 2 A lattice model with nonsymmorphic symmetry in the momentum space. **a** The flux configuration and gauge connections of a lattice model. The chosen unit cell is specified by the green dashed rectangle. The blue shaded regions respect M_x and have a unit lattice length along the y direction. Both of them have a net flux $\pi \bmod 2\pi$. **b** The gauge transformation to restore the original gauge connections after reflection M_x .

nonsymmorphic symmetries are fundamentally distinct from the momentum-space nonsymmorphic symmetry M_x discovered here, for which the fractional translation acts in momentum space. It is also clear that M_x is a free operation, i.e., no momentum is invariant under M_x . The emergence of momentum-space nonsymmorphic symmetry is a unique feature of projective symmetry algebras. The free character of such symmetry operations will produce remarkable consequences, as we discuss below.

Brillouin Klein bottle. We proceed to elucidate the physical consequences of this momentum-space glide reflection symmetry. Let $\mathcal{H}(\mathbf{k})$ be the Bloch Hamiltonian in momentum space. Then, the constraint by M_x in Eq. (3) is

$$U\mathcal{H}(k_x, k_y)U^\dagger = \mathcal{H}(-k_x, k_y + \pi). \tag{5}$$

Here, for simplicity we have set $b = 1$. This means if $|\psi(\mathbf{k})\rangle$ is an eigenstate of $\mathcal{H}(\mathbf{k})$ with energy $\mathcal{E}(\mathbf{k})$, then $U|\psi(\mathbf{k})\rangle$ will be an eigenstate of $\mathcal{H}(-k_x, k_y + \pi)$ with the same energy, i.e.,

$$\mathcal{H}(-k_x, k_y + \pi)U|\psi(\mathbf{k})\rangle = \mathcal{E}(\mathbf{k})U|\psi(\mathbf{k})\rangle. \tag{6}$$

As a result the spectrum at (k_x, k_y) is equivalent to that at $(-k_x, k_y + \pi)$. Thus, the Brillouin zone can be partitioned into two parts, $\tau_{1/2}$ and $\bar{\tau}_{1/2}$, as illustrated in Fig. 3a. Only one of them is independent, i.e., the fundamental domain of momentum space is a half of the Brillouin zone.

This can be explicitly verified for the model in Fig. 2. In Fig. 3d, we plot the spectrum of the lattice model. One can observe that the reflection of the band structure over $\tau_{1/2}$ through the k_y axis coincides with that over $\bar{\tau}_{1/2}$ after a half translation $\mathcal{L}_{G_y/2}$. This can be more clearly seen from the constant energy cut in Fig. 3e.

We have emphasized that as a momentum-space nonsymmorphic symmetry, M_x is a free operation with no fixed point, distinct from conventional space group symmetries. Mathematically, it is known that an equivariant bundle with the structure group G freely acting on the based space X is equivalent to the bundle on the orbital space X/G ²⁷. For our case, this simply means all the information including topology is fully captured by the fundamental domain $\tau_{1/2} = [-\pi, \pi) \times [-\pi, 0)$. Since k_x is periodic, we may write $\tau_{1/2} = S^1 \times [-\pi, 0)$ as a cylinder. This cylinder has two boundaries S^1_\pm at $k_y = -\pi$ and 0 , respectively. Importantly, S^1_\pm are oppositely oriented and “glued” together, because they are connected by M_x [Fig. 3b]. Thus, the fundamental domain here is topologically a Klein bottle, as illustrated in Fig. 3c.

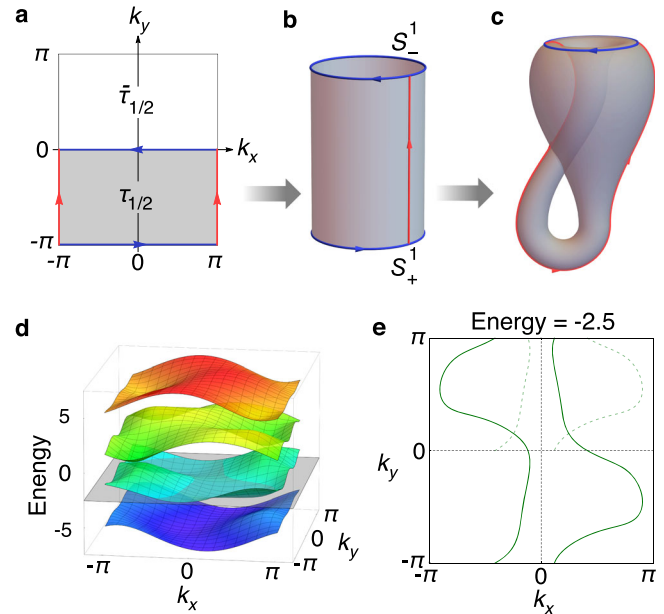


Fig. 3 Momentum space representation of the symmetry and Brillouin Klein bottle. **a** The fundamental domain of the Brillouin zone is $\tau_{1/2}$. The boundaries with the same color should be identified along the marked direction. **b** The cylinder with two boundaries S^1_\pm identified along opposite directions, which is essentially the Brillouin Klein bottle in **c**. **d** Energy bands of the model in Fig. 2a. **e** A constant energy cut, which corresponds to the gray colored plane in **d**. The reflection of the band structure over $\tau_{1/2}$ through the k_y axis coincides with that over $\bar{\tau}_{1/2}$ after a half translation $\mathcal{L}_{G_y/2}$. For comparison, in **e** the curves within $\tau_{1/2}$ are translated to $\bar{\tau}_{1/2}$, and marked as light dashed green lines.

We remark that in solid state physics, conventional space group symmetries are commonly used to reduce Brillouin zones to so-called irreducible Brillouin zones. However, because those symmetries are not free, the irreducible Brillouin zone is not sufficient to capture the topological information (e.g., symmetry information is still required at high-symmetry points or paths of the irreducible Brillouin zone), distinct from the case here. Besides, the Brillouin Klein bottle is a closed manifold, whereas the irreducible Brillouin zones are not. These characters are important for the topological classification to be discussed in the following.

Topological invariant and edge states. Consider the system is in an insulating phase. The task of topological classification is to classify valence-band wave functions (forming a Hermitian vector bundle) over the Brillouin Klein bottle. This is fundamentally different from the usual cases where the base manifold is a torus or a sphere. A crucial difference is the orientability. A torus (and a sphere) is orientable, whereas a Klein bottle is non-orientable. For orientable closed base manifolds such as the torus, the most elementary topological invariant is the Chern number, which is the integration of the Berry curvature \mathcal{F} for valence bands over the Brillouin torus. The Chern number is valued in \mathbb{Z} , and the sign of the integer is related to the orientation of the torus, since a reflection inverts the Chern number. In contrast, for the Brillouin Klein bottle that is non-orientable, any topological invariant can only be valued in \mathbb{Z}_2 , since the sign of the invariant has no significance and we must have $1 = -1$.

Now, we formulate an explicit expression for this \mathbb{Z}_2 topological invariant. This is based on two key observations. First, the two boundaries S^1_\pm of $\tau_{1/2}$ are related by an inversion of k_x [Fig. 3a]. The inversion operation inverts the Berry phase

for a 1D system²⁸. Hence, the Berry phases $\gamma(-\pi)$ and $\gamma(0)$ over S^1_{\pm} are opposite up to an multiple of 2π , i.e., $\gamma(0) + \gamma(-\pi) = 0 \pmod{2\pi}$. Second, due to Stoke's theorem, $\int_{\tau_{1/2}} d^2k \mathcal{F} + \gamma(0) - \gamma(-\pi) = 0 \pmod{2\pi}$. Therefore, we can formulate the \mathbb{Z}_2 invariant as

$$\nu = \frac{1}{2\pi} \int_{\tau_{1/2}} d^2k \mathcal{F} + \frac{1}{\pi} \gamma(0) \pmod{2}. \tag{7}$$

Here, the formula is valued in integers because of the two observations above. Since a large gauge transformation for valence wave functions can change $\gamma(0)$ by a multiple of 2π , only the parity of the formula is gauge invariant and hence can be defined as a topological invariant. We also comment that the \mathbb{Z}_2 topological classification here is based on the equivariant K theory or KG theory by $\bar{K}(K) = \mathbb{Z}_2$, where K is the Klein bottle. The topological invariant is derived from the fact that line bundles over a 2D manifold M are topologically classified by $H^2(M, \mathbb{Z})$, with $H^2(K, \mathbb{Z}) = \mathbb{Z}_2$. Thus the resultant classification and the topological invariant are stable under the addition of trivial bands.

We can give Eq. (7) a pump interpretation with an intuitive geometric picture. Over $\tau_{1/2} = S^1 \times [-\pi, 0]$, we can always choose a complete set of continuous valence states $|\psi_n(\mathbf{k})\rangle$, which are periodic along k_x . Then, the corresponding Berry connection $\mathcal{A}(\mathbf{k})$ is also periodic in k_x . For such a $\mathcal{A}(\mathbf{k})$, we can compute $\gamma(k_y)$ that is continuous from $k_y = -\pi$ to 0. Moreover, it is straightforward to derive that $\int_{\tau_{1/2}} d^2k \mathcal{F} = -\int_{-\pi}^0 dk_y \partial_{k_y} \gamma(k_y) = \gamma(-\pi) - \gamma(0)$. Hence, from Eq. (7), we find that

$$\nu = \frac{1}{2\pi} [\gamma(0) + \gamma(-\pi)] \pmod{2}. \tag{8}$$

Considering the generic case that $\gamma(-\pi) \neq 0$ or π , the path of $\gamma(k_y)$ has to cross 0 or π in the course of varying k_y from $-\pi$ to 0 [see Fig. 4a]. Introducing $W_{0/\pi}$ as the number of times that $\gamma(k_y)$ crosses $0/\pi$, ν can be given a geometric interpretation:

$$\nu = W_{\pi} \pmod{2}, \tag{9}$$

i.e., ν is nontrivial if and only if $\gamma(k_y)$ crosses π an odd number of times.

The insulator with nontrivial $\nu = 1$ may be termed as a Klein bottle insulator. It features special topological edge states, whose existence can be understood from Eq. (9). For nontrivial ν , $\gamma(k_y)$ has to cross π at some (odd number of) k_y , then the 1D k_x -subsystems at these crossing points have Berry phases of π . It is well known that the valence-band Berry phase correspond to the center of Wannier function and the 1D charge polarization. Particularly, $\gamma = \pi$ corresponds to Wannier center at the midpoints between lattice sites, and therefore leads to an in-gap state at each end. Thus, there must be in-gap boundary states located at each edge parallel to the y direction. Because of the continuity of energy bands, these in-gap states must be connected to form a topological edge band.

Consider our model in Fig. 2 with two sets of parameters. The topological invariant Eq. (9) is computed as shown in Fig. 4b, c, respectively. The corresponding band structures for a ribbon geometry with edges along the y direction, are shown in Fig. 4d, e. The topological edge bands are clearly observed for the Klein bottle insulator phase with $\nu = 1$. Similar to the Möbius insulators, these edge bands are detached from the bulk bands^{19,29,30}. Under strong boundary potentials, they could be shifted out of the gap.

We note two features of the edge states that distinguish the Klein bottle insulator from conventional crystalline topological insulators. First, the gapless modes appear on mirror-symmetry-

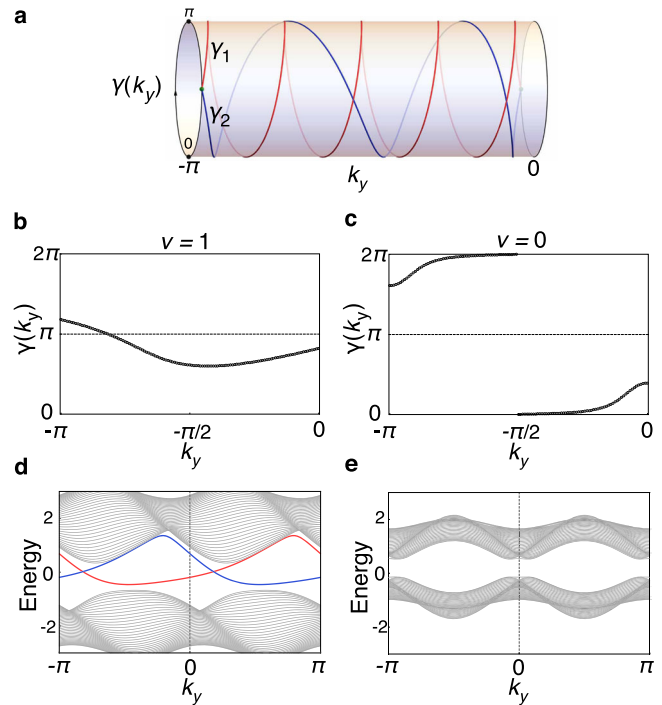


Fig. 4 Topological invariant and edge states. **a** Schematic illustration of the formula in Eq. (9). The red and blue paths correspond to the topologically nontrivial and trivial cases, respectively. **b** and **c** depict the flows of $\gamma(k_y)$ for two set of parameters for the model in Fig. 2a, and the corresponding band structures on a ribbon geometry with edges along y are given in **d** and **e**, respectively. States on right/left edge are marked in red/blue color.

breaking edges, rather than on symmetry-preserving edges as for conventional crystalline topological insulators. It is easy to see that the above argument indicates the existence of topological edge modes on any edge not perpendicular to y , whereas the mirror-symmetric edge perpendicular to y is expected to be gapped without topological edge mode. Second, the momentum-space glide reflection fascinatingly leads to a nonlocal relation for edge states. Consider two edges along y connected by the M_x symmetry in real space. Because of the nonsymmorphic character of M_x in the momentum space, only the energy bands over $k_y \in [-\pi, 0)$ are independent, while those over $k_y \in [0, \pi)$ can be deduced from the action of M_x . Particularly, M_x nonlocally maps the topological edge band on one edge over $k_y \in [-\pi, 0)$ to that on the other edge over $k_y \in [0, \pi)$. In Fig. 4d, one can clearly see that translating the edge band on the left edge by $G_y/2$ coincides with that on the right edge.

We have demonstrated that interplay between gauge fields and symmetry can fundamentally modify the Bloch band theory. Under gauge fields, a spatial symmetry can acquire a nonsymmorphic character in momentum space. Particularly, the momentum-space glide reflection can reduce the Brillouin torus to the Brillouin Klein bottle, and therefore change the topological classifications from the bottom level. We formulate a novel kind of topological insulator over the Brillouin Klein bottle, which is as elementary as the Chern insulator over the Brillouin torus. Although we take 2D reflection in our analysis, the discussion can be readily generalized to the 3D with analogous momentum-space glide reflections and screw rotations (see Supplementary Note 4 for demonstrations). Since glide reflection and screw rotations are the most elementary nonsymmorphic symmetries, all nonsymmorphic space groups may be realized on the reciprocal lattices by certain gauge flux configurations, which

are mathematically dictated by the second cohomology groups of the space groups. Since gauge fluxes can be engineered in artificial crystals for realizing projective symmetries^{23,24}, our work opens the door toward a fertile ground for exploring novel momentum-space symmetries and topologies of artificial crystals beyond the scope of topological quantum materials.

Methods

The simple 2D model. We consider a model defined on the rectangular lattice in Fig. 2. Constrained by M_x and two translation symmetries, the most general Hamiltonian with only nearest neighbor hopping terms is given by

$$\mathcal{H}_0(\mathbf{k}) = \begin{bmatrix} \varepsilon & [q_1^x(k_x)]^* & [q_+^y(k_y)]^* & 0 \\ q_1^x(k_x) & \varepsilon & 0 & [q_-^y(k_y)]^* \\ q_+^y(k_y) & 0 & -\varepsilon & [q_2^x(k_x)]^* \\ 0 & q_-^y(k_y) & q_2^x(k_x) & -\varepsilon \end{bmatrix}, \quad (10)$$

where $q_a^x(k_x) = t_{a1}^x + t_{a2}^x e^{ik_x}$ with $a = 1, 2$, $q_{\pm}^y(k_y) = t_1^y \pm t_2^y e^{ik_y}$, $\pm\varepsilon$ are on-site energies. To break the time-reversal (T) symmetry, we may include the following second neighbor hopping terms, $\mathcal{H}^{(1)}(\mathbf{k}) = \lambda \cos k_y \tau_1 \otimes \sigma_2 + \lambda \sin k_y \tau_2 \otimes \sigma_2$. For Figs. 3d, e and 4b, d, the parameter are given by $t_{11}^x = t_{22}^x = 1$, $t_{12}^x = t_{21}^x = 3.5$, $t_1^y = 2$, $t_2^y = 1.5$, $\varepsilon = 1$, $\lambda = 1$. For Fig. 4c, e, $t_{11}^x = t_{12}^x = 1$, $t_{21}^x = 3.5$, $t_{22}^x = 1.7$, $t_1^y = 2$, $t_2^y = 1.5$, $\varepsilon = 0.6$, $\lambda = 0$.

It is worth pointing out that if the T symmetry is preserved, the two 1D k_x -subsystems $\mathcal{H}(k_x, \pm\pi/2)$ are invariant under $M_x T$. This is because T inverts $(k_x, \pm\pi/2)$ to $(-k_x, \mp\pi/2)$, but M_x moves $(-k_x, \mp\pi/2)$ back to $(k_x, \pm\pi/2)$. Then, $M_x T$ is effectively a spacetime inversion symmetry for $\mathcal{H}(k_x, \pm\pi/2)$, and therefore can quantize its Berry phases into integral multiples of π . As a result, the curve in Fig. 4b would always cross π at $k_y = -\pi/2$.

Data availability

The data generated and analyzed during this study are available from the corresponding author upon reasonable request.

Received: 8 October 2021; Accepted: 10 April 2022;

Published online: 25 April 2022

References

- Thouless, D. J., Kohmoto, M., Nightingale, M. P. & den Nijs, M. Quantized hall conductance in a two-dimensional periodic potential. *Phys. Rev. Lett.* **49**, 405–408 (1982).
- Simon, B. Holonomy, the quantum adiabatic theorem, and berry's phase. *Phys. Rev. Lett.* **51**, 2167–2170 (1983).
- Chiu, C.-K., Teo, J. C. Y., Schnyder, A. P. & Ryu, S. Classification of topological quantum matter with symmetries. *Rev. Mod. Phys.* **88**, 035005 (2016).
- Volovik, G. E. *The Universe in a Helium Droplet*, Vol. 117 (Oxford University Press on Demand, 2003).
- Qi, X.-L. & Zhang, S.-C. Topological insulators and superconductors. *Rev. Mod. Phys.* **83**, 1057–1110 (2011).
- Hasan, M. Z. & Kane, C. L. Colloquium: topological insulators. *Rev. Mod. Phys.* **82**, 3045–3067 (2010).
- Ozawa, T. et al. Topological photonics. *Rev. Mod. Phys.* **91**, 015006 (2019).
- Ma, G., Xiao, M. & Chan, C. T. Topological phases in acoustic and mechanical systems. *Nat. Rev. Phys.* **1**, 281–294 (2019).
- Lu, L., Joannopoulos, J. D. & Soljačić, M. Topological photonics. *Nat. Photonics* **8**, 821–829 (2014).
- Yang, Z. et al. Topological acoustics. *Phys. Rev. Lett.* **114**, 114301 (2015).
- Xue, H. et al. Observation of an acoustic octupole topological insulator. *Nat. Commun.* **11**, 2442 (2020).
- Imhof, S. et al. Topoelectrical-circuit realization of topological corner modes. *Nat. Phys.* **14**, 925–929 (2018).
- Yu, R., Zhao, Y. X. & Schnyder, A. P. 4d spinless topological insulator in a periodic electric circuit. *Nat. Sci. Rev.* **7**, 1288–1295 (2020).
- Prodan, E. & Prodan, C. Topological phonon modes and their role in dynamic instability of microtubules. *Phys. Rev. Lett.* **103**, 248101 (2009).
- Huber, S. D. Topological mechanics. *Nat. Phys.* **12**, 621–623 (2016).
- Cooper, N. R., Dalibard, J. & Spielman, I. B. Topological bands for ultracold atoms. *Rev. Mod. Phys.* **91**, 015005 (2019).

- Dalibard, J., Gerbier, F., Juzeliūnas, G. & Öhberg, P. Colloquium: artificial gauge potentials for neutral atoms. *Rev. Mod. Phys.* **83**, 1523 (2011).
- Wen, X.-G. Quantum orders and symmetric spin liquids. *Phys. Rev. B* **65**, 165113 (2002).
- Zhao, Y. X., Huang, Y.-X. & Yang, S. A. \mathbb{Z}_2 -projective translational symmetry protected topological phases. *Phys. Rev. B* **102**, 161117(R) (2020).
- Zhao, Y. X., Chen, C., Sheng, X.-L. & Yang, S. A. Switching spinless and spinful topological phases with projective PT symmetry. *Phys. Rev. Lett.* **126**, 196402 (2021).
- Shao, L. B., Liu, Q., Xiao, R., Yang, S. A. & Zhao, Y. X. Gauge-field extended $k \cdot p$ method and novel topological phases. *Phys. Rev. Lett.* **127**, 076401 (2021).
- Bradley, C. & Cracknell, A. *The Mathematical Theory of Symmetry in Solids: Representation Theory for Point Groups and Space Groups* (Oxford University Press, 2009).
- Xue, H. et al. Projectively enriched symmetry and topology in acoustic crystals. *Phys. Rev. Lett.* **128**, 116802 (2022).
- Li, T. et al. Acoustic Möbius insulators from projective symmetry. *Phys. Rev. Lett.* **128**, 116803 (2022).
- Wieder, B. J. & Kane, C. L. Spin-orbit semimetals in the layer groups. *Phys. Rev. B* **94**, 155108 (2016).
- Watanabe, H., Po, H. C., Vishwanath, A. & Zaletel, M. Filling constraints for spin-orbit coupled insulators in symmorphic and nonsymmorphic crystals. *Proc. Natl Acad. Sci. USA* **112**, 14551–14556 (2015).
- Segal, G. Equivariant K-theory. *Publ. Math. ématiques de l'IHÉS* **34**, 129–151 (1968).
- Zak, J. Berry's phase for energy bands in solids. *Phys. Rev. Lett.* **62**, 2747–2750 (1989).
- Shiozaki, K., Sato, M. & Gomi, K. \mathbb{Z}_2 topology in nonsymmorphic crystalline insulators: Möbius twist in surface states. *Phys. Rev. B* **91**, 155120 (2015).
- Young, S. M. & Wieder, B. J. Filling-enforced magnetic dirac semimetals in two dimensions. *Phys. Rev. Lett.* **118**, 186401 (2017).

Acknowledgements

This work is supported by National Natural Science Foundation of China (Grants No. 12174181, No. 12161160315, and No. 11874201), and the Singapore MOE AcRF Tier 2 (MOE2019-T2-1-001).

Author contributions

Z.Y.C. and Y.X.Z. conceived the idea. S.A.Y. and Y.X.Z. supervised the project. Z.Y.C. and Y.X.Z. did the theoretical analysis. Z.Y.C., S.A.Y. and Y.X.Z. wrote the manuscript.

Competing interests

The authors declare no competing interests.

Additional information

Supplementary information The online version contains supplementary material available at <https://doi.org/10.1038/s41467-022-29953-7>.

Correspondence and requests for materials should be addressed to Y. X. Zhao.

Peer review information *Nature Communications* thanks the anonymous, reviewer(s) for their contribution to the peer review of this work.

Reprints and permission information is available at <http://www.nature.com/reprints>

Publisher's note Springer Nature remains neutral with regard to jurisdictional claims in published maps and institutional affiliations.



Open Access This article is licensed under a Creative Commons Attribution 4.0 International License, which permits use, sharing, adaptation, distribution and reproduction in any medium or format, as long as you give appropriate credit to the original author(s) and the source, provide a link to the Creative Commons license, and indicate if changes were made. The images or other third party material in this article are included in the article's Creative Commons license, unless indicated otherwise in a credit line to the material. If material is not included in the article's Creative Commons license and your intended use is not permitted by statutory regulation or exceeds the permitted use, you will need to obtain permission directly from the copyright holder. To view a copy of this license, visit <http://creativecommons.org/licenses/by/4.0/>.

© The Author(s) 2022